# Arctic-wide sea ice thickness estimates from combining satellite remote sensing data and a dynamic ice-ocean model with data assimilation during the CryoSat-2 period

**Longjiang Mu[1,2], Martin Losch[2], Qinghua Yang[1], Robert Ricker[2], Svetlana N. Losa[2,3], and Lars Nerger[2]**

[1]Guangdong Province Key Laboratory for Climate Change and Natural Disaster Studies, and School of Atmospheric Sciences, Sun Yat-sen University, Zhuhai, China

[2]Alfred Wegener Institute, Helmholtz Centre for Polar and Marine Research, Bremerhaven, Germany

[3]Shirshov Institute of Oceanology, Russian Academy of Sciences, Moscow, Russia

**Key Points:**

- A new Arctic sea ice thickness record is generated by assimilating CryoSat-2 and SMOS thickness products simultaneously.
- The new sea ice thickness are close to satellite data in freezing seasons and further cover the summer seasons.
- Comparisons with in-situ observations show the new record has some advantages over PIOMAS and CS2SMOS thickness.

Corresponding author: Qinghua Yang, `yangqh25@mail.sysu.edu.cn`

Corresponding author: Longjiang Mu, `longjiang.mu@awi.de`

**Abstract**

Exploiting the complementary character of CryoSat-2 and Soil Moisture and Ocean Salinity (SMOS) satellite sea ice thickness products, daily Arctic sea ice thickness estimates from October 2010 to December 2016 are generated by an Arctic regional ice-ocean model with satellite thickness assimilated. The assimilation is performed by a Local Error Subspace Transform Kalman filter (LESTKF) coded in the Parallel Data Assimilation Framework (PDAF). The new estimates can be generally thought of as combined model and satellite thickness (CMST). It combines the skill of satellite thickness assimilation in the freezing season and with the skill of model dynamics in the melting season, thus further fills the gaps in thickness data during the melting season when neither CryoSat-2 nor SMOS sea ice thickness is available. Comparisons with in-situ observations from the Beaufort Gyre Exploration Project (BGEP), Ice Mass Balance (IMB) Buoys and the NASA Operation IceBridge demonstrate that CMST reproduces most of the observed temporal and spatial variations. Results also show that CMST is comparable to the Pan-Arctic Ice Ocean Modeling and Assimilation System (PIOMAS) product, and appears to correct some thickness biases where PIOMAS overestimates in thin ice areas and underestimates in thick ice areas. Due to imperfect parameterizations in the sea ice model and satellite thickness retrievals, CMST does not reproduce the heavily deformed and ridged sea ice along the northern coast of the Canadian Arctic Archipelago (CAA) and Greenland. With the new Arctic sea ice thickness estimates sea ice volume changes in recent years can be further assessed.

## 1 Introduction

Arctic sea ice extent as an indicator of climate change has been monitored by satellites for decades. On the one hand, the linkages between the Arctic ice extent and mid-latitude climate have been documented several times (Francis et al., 2009; Kumar et al., 2010; Liu et al., 2012; Overland & Wang, 2010; Serreze et al., 2007). On the other hand, sea ice thickness may be a more important observable than extent or concentration because it is more directly related to sea ice volume. It is, however, more difficult to observe from space. The sparsity of thickness data results in an incomplete closure of the surface energy and freshwater budgets in the Arctic Ocean (Haine et al., 2015). There are ongoing efforts to construct consistent time series of Arctic sea ice thickness from satellite remote sensing data. Freeboard measurements by satellite altimeters on the Ice, Cloud, and land Elevation Satellite (ICESat) and CryoSat-2 can be used to obtain sea ice thickness estimates assuming hydrostatic equilibrium (Kwok et al., 2009; Laxon et al., 2013). Thin ice thickness can be retrieved by exploiting the brightness temperature observations at the L-band frequency of 1.4 GHz from the Soil Moisture Ocean Salinity (SMOS) satellite (Tian-Kunze et al., 2014). To bridge the gap between ICESat and ICESat-2 (scheduled for launch in 2018), the NASA IceBridge airborne campaigns are conducted every year in spring from 2009 providing valuable information of ice and snow thickness in different regions of the Western Arctic (Kurtz et al., 2013). This airborne data record can also be used for validation of satellite-derived sea ice thickness.

Often, retrieval algorithms result in large uncertainties in derived satellite data products. There are different assumptions for snow loading and empirical parameters as well as intrinsic limitations of different satellite sensors (radar/laser altimetry, radiometry) so that there can be large differences between different products (Wang et al., 2016). The uncertainties of different products also differ depending on the used methods and the properties of the sensed ice cover. In spite of these uncertainties, satellite data products resolve ice thickness changes on basin and regional scales. In addition, uncertainties can be reduced by combining different ice thickness data products. For example, the complementary character of the uncertainties in CryoSat-2 and SMOS ice thickness products makes it possible to combine the data with an optimal interpolation scheme into a merged product CS2SMOS with better spatial and temporal coverage than the individual data sets (Ricker et al., 2017). With this combination the overall uncertainties in Arctic sea ice thickness can be reduced by implementing the individual advantages of each product. The CS2SMOS dataset covers the entire Arctic and provides ice thickness and the related uncertainties during the freezing season. The drawbacks of the CS2SMOS dataset are that the data is not available during the melt season in spring and summer and that the optimal interpolation method is purely statistical and does not contain any information from physical processes (Mu et al., 2018).

For a continuous long-term ice thickness record, numerical model estimates can be used to fill the gaps in the satellite products, especially during summer. The Pan-Arctic Ice-Ocean Modeling and Assimilation System (PIOMAS) provides sea ice thickness and volume records that have been evaluated and tuned with submarine data and ICESat derived ice thickness (Zhang & Rothrock, 2003; Schweiger et al., 2011). PIOMAS data have become a reference dataset especially for thickness time series in the Arctic, but the data appear to overestimate thin ice thickness in the Beaufort Sea and underestimate thick ice around the Canadian Arctic Archipelago (CAA) area compared to IceBridge thickness(Wang et al., 2016). Assimilating sea ice thickness data from satellite-based remote sensing is expected to reduce these sea ice thickness biases in the model. For example, Lisæter et al. (2007) showed in idealized experiments with synthetic CryoSat data that sea ice and ocean state variables improve with sea ice thickness data assimilation. A series of studies also showed that the assimilation of SMOS ice thickness significantly improves the first-year ice estimates (Yang et al., 2014, 2016b; Xie et al., 2016). Assimilating CryoSat-2 ice thickness data in addition to SMOS ice thickness into an ice-ocean model in the cold season lead to a reliable pan-Arctic sea ice thickness estimate that is consistent with in-situ observations (Mu et al., 2018) .

Both SMOS and CryoSat-2 thickness retrieval algorithms fail in the presence of water on the ice, for example in melt ponds, so that these data are restricted to the cold season. To include the melting season, we extend the study of Mu et al. (2018) to cover the entire CryoSat-2 period from October 2010 to December 2016. The weekly averaged CryoSat-2 ice thickness is assimilated into the model in addition to the daily Special Sensor Microwave Imager Sounder (SSMIS) sea ice concentration and SMOS sea ice thickness data. The sea ice thickness assimilated in the freezing season is expected to provide a good initial state for sea ice thickness in the melt season when thickness data are not available (Day et al., 2014). The assimilated sea ice concentration in summer has some potential to correct potential sea ice thickness biases by means of their covariance (Yang et al., 2015a, 2015b, 2016a). Therefore, the new dataset is expected to cover the entire Arctic without the temporal gaps in CS2SMOS and with satellite sea ice thickness information that is not included in PIOMAS.

The paper is organized as follows: In section 2, we describe the satellite-based sea ice thickness observations, model and in-situ measurements that are used for assimilation and evaluation. In section 3, we detail the method to establish our model thickness estimates. The evaluation metrics and comparisons between different products and in-situ observations are presented in section 4. The results are discussed in section 5 and conclusions are drawn in section 6.

# 2 Sea Ice Thickness Data

## 2.1 Soil Moisture Ocean Salinity (SMOS) Thickness Data

The SMOS satellite was launched by the European Space Agency (ESA) in 2009 and provides brightness temperature. A thermodynamic sea ice model and a single-layer emissivity model are used to retrieve ice thickness from the brightness temperature (Tian-Kunze et al., 2014). A daily ice thickness product with a spatial resolution of 12.5 km on the National Snow and Ice Data Center (NSIDC) polar-stereographic grid projection is available at the Integrated Climate Data Center (ICDC) at the University of Hamburg (`http://icdc.cen.uni-hamburg.de/`). Because of the specific assumptions of the retrieval algorithm, data with an uncertainty $> 1$ m or with a ratio between retrieved and maximum retrievable sea ice thickness near 100% are flagged and not used. In practice, this means that only the SMOS data with thickness $< 1$ m are used for assimilation.

In this study, the SMOS v3.1 ice thickness data are used covering the period 2010-2016. The daily product also contains uncertainty estimates. These are used as assumed observation errors during the data assimilation. Data and uncertainties are linearly interpolated onto the model grid.

## 2.2 CryoSat-2 Thickness Data

CryoSat-2, also launched by the ESA in 2010, is dedicated to retrieve thickness of perennial sea ice (Wingham et al., 2006). The thickness data are derived from sea ice freeboard data, which are obtained from radar altimeter range measurements. Assuming hydrostatic equilibrium and employing a pragmatic approach on snow loading (Laxon et al., 2013), freeboard can be converted into sea ice thickness. The relative uncertainties are smaller for thick ice than for thin ice because of the relatively larger freeboard of thick ice (Ricker et al., 2014).

Weekly CryoSat-2 ice thickness data from the Alfred Wegener Institute (AWI), Helmholtz Centre for Polar and Marine Research are available for the period 2010–2016 (Ricker et al., 2014, `http://data.meereisportal.de`). This dataset is available on the EASE-Grid 2.0 (Brodzik et al., 2012) with a grid resolution of 25 km. It is then interpolated to our model grid. The uncertainties provided with the data are also used as the assumed observation errors during data assimilation. However, due to the 30 day sub-cycle of CryoSat-2, weekly means of ice thickness have significant data gaps where orbit coverage is incomplete.

### 2.3 CS2SMOS

The complementarity of the data coverage as well as the sea ice thickness uncertainties between CryoSat-2 and SMOS inspired a statistically merged product (CS2SMOS) (Ricker et al., 2017, `http://data.meereisportal.de`). The weekly CS2SMOS sea ice thickness data cover the entire Arctic including the North Pole and are projected onto the 25 km EASE-Grid 2.0. Compared to airborne thickness data, CS2SMOS represents an improvement over CryoSat-2 thickness in the thin ice regimes. CS2SMOS thicknesses also have a low bias in the mixed first-year and multi-year ice regimes. The uncertainties provided in the dataset can be used to approximate the data error statistics. In this study, the CS2SMOS v1.3 ice thickness product is used for comparison. The data are interpolated bi-linearly onto the model grid.

### 2.4 Pan-Arctic Ice Ocean Modeling and Assimilation System (PIOMAS)

The PIOMAS (Zhang & Rothrock, 2003) consists of the Parallel Ocean Program (POP) and a 12-category thickness and enthalpy distribution sea ice model. The system is forced by 10 m surface winds, 2 m surface air temperature, cloud cover, downwelling longwave radiation, specific humidity, precipitation, evaporation and sea level pressure from an NCEP/NCAR reanalysis. Sea ice concentration from the NSIDC near-real time product and sea surface temperature (SST) from the NCEP/NCAR Reanalysis are introduced into the system by nudging and optimal interpolation (Zhang & Rothrock, 2003; Schweiger et al., 2011). Daily sea ice thickness estimates are provided from 1978 to present on the PIOMAS grid (`http://psc.apl.uw.edu/data/`). In this study, the PIOMAS v2.1 ice thickness data set is used for comparison.

### 2.5 Beaufort Gyre Exploration Project (BGEP)

Starting in 2003, the Beaufort Gyre Exploration Project based at the Woods Hole Oceanographic Institution (BGEP, `http://www.whoi.edu/beaufortgyre`) deploys upward-looking sonar (ULS) moorings every year at three locations BGEP_A, BGEP_B and BGEP_D

(Figure 4). The ULS can measure the ice draft with an error of about 0.1 m (Melling et al., 1995). Drafts are converted to thickness by multiplying with a factor of 1.1 that is calculated as the ratio of the mean seawater and sea ice densities (Nguyen et al., 2011). Note that this draft-thickness conversion is very simple. The uncertainties caused by the absence of sufficient information about different ice types, ice densities, and snow loading are ignored in the study. In contrast to the IceBridge thickness data (section 2.7), the BGEP long-term ice thickness observations provide a year-round reference for the comparisons between different ice thickness products.

### 2.6 Ice Mass Balance (IMB) Buoys

IMB buoys have been deployed for more than two decades and provide a comprehensive Lagrangian dataset on sea ice evolution along their drift trajectories (Perovich et al., 2009, `http://imb-crrel-dartmouth.org`). The acoustic sounder above ice and the underwater sonar altimeter below ice autonomously measure the ice growth and ablation. The uncertainty of sea ice thickness measured by each acoustic sounder is within 5 mm (Richter-Menge et al., 2006). These long-term (some buoys collected data for nearly two years) and consistent observations of sea ice thickness support the evaluation of different sea ice thickness products.

The deployment positions of IMB buoys are considered strategically for some key locations or in collocation with other instruments. Note that, generally, IMB buoys tend to be deployed on thick and level ice floes to achieve the longest possible time series. As a consequence, comparing the Lagrangian observed thickness and the Eulerian model estimates is not entirely consistent and can be ambiguous.

### 2.7 Operation IceBridge

NASA's Operation IceBridge (`https://www.nasa.gov/mission_pages/icebridge/`) conducts airborne surveys on polar ice in the Arctic and Antarctic. On these flights, a Snow Radar and the Airborne Topographic Mapper (ATM) onboard the aircraft monitors snow and ice thickness (Kurtz et al., 2013) of ice sheets, ice shelves and sea ice to bridge the gap between ICESat and ICESat-2 since 2009.

We use IceBridge sea ice thickness data from 2011 to 2013 obtained from IceBridge L4 Sea Ice Freeboard, Snow Depth, and Thickness (IDCSI4) data set, Version 1 (Kurtz et al., 2015, `http://nsidc.org/data/idcsi4`). An experimental Quicklook product of IceBridge thickness from 2012 to 2016 are not used because of the potentially larger uncertainties. The sea ice thickness data and their uncertainties in IDCSI4 are estimated over a 40 m length scale. The IceBridge campaigns for the Arctic conducted during March and April provide valuable estimates of approximate maximum ice thickness of the year.

## 3 The Model Sea Ice Thickness Estimates

### 3.1 The Arctic Regional Sea Ice-Ocean Model

We use a regional, pan-Arctic sea ice-ocean model (Losch et al., 2010; Nguyen et al., 2011; Yang et al., 2014; Mu et al., 2017) based on the Massachusetts Institute of Technology general circulation model (MITgcm, Marshall et al., 1997). The sea ice dynamics use a viscous plastics rheology (Hibler III, 1979; Zhang & Hibler, 1997). The sea ice thermodynamics use a one-layer, zero heat capacity formulation (Semtner Jr, 1976; Parkinson & Washington, 1979). The sea ice package in the MITgcm also provides an ice thickness distribution (ITD) model (Ungermann et al., 2017). We do not use the ITD model because the redistribution of the ice thickness in different categories under sea ice thickness assimilation is not straightforward. Snow thickness is a prognostic variable following Zhang et al. (1998). The model sea ice thickness estimates are grid-cell averaged ice thickness. This quantity is also called effective ice thickness (Schweiger et al., 2011). Both the ocean and sea ice model are discretized on an Arakawa C grid with a grid spacing of 18 km. In the vertical direction, there are 50 unevenly spaced layers in the ocean model to resolve the halocline in the Arctic Ocean. The bathymetry is derived from the National Centers for Environmental Information (formerly the National Geophysical Data Center (NGDC)) 2-minute gridded elevations/bathymetry for the world (ETOPO2, Smith & Sandwell, 1997). A global model (Menemenlis et al., 2008) provides monthly oceanic boundary conditions for the regional model. Model parameters for sea ice and ocean were optimized by Nguyen et al. (2011) using a Green function method and further tuned in this study. The albedos for sea ice are set to 0.75 and 0.56 for dry or wet conditions, and those for snow are set to 0.84 and 0.70. Additional important parameters are the lead closing parameter $Ho = 0.6074$ and the sea ice strength parameter $P^* = 2.264\times10^4\,\mathrm{Nm}^{-2}$. The ocean model uses free-slip lateral boundary conditions, while for the sea ice model no-slip lateral conditions are applied. For more details of the model configuration the reader is referred to Losch et al. (2010) and Nguyen et al. (2011).

### 3.2 Atmospheric Forcing

Following Yang et al. (2015a) and Mu et al. (2018), the atmospheric ensemble forecasts of the United Kingdom Met Office (UKMO) Ensemble Prediction System (EPS) (Bowler et al., 2008) available in the TIGGE archive (`http://tigge.ecmwf.int`) are used to drive the ice-ocean model. There are 23 ensemble members during 1 January 2010 to 15 July 2014, and 11 ensemble members during 6 November 2014 to 31 December 2016, because the ensemble of UKMO EPS changed from MOGREPS-15 version 14 (UM version 8.3) to MOGREPS-G version 15 (UM version 8.5) with a reduced number of ensemble members but with higher horizontal resolution (from N216 to N400). Unfortunately, there is no UKMO EPS ensemble during this transition from 16 July 2014 to 5 November 2014. The UKMO EPS uses an Ensemble Transform Kalman Filter (ETKF) and the scheme of Shutts (2005) to take into account the initial uncertainties and the effect of model uncertainties (Bowler et al., 2008). The ensemble forecasts have been shown to effectively represent the atmospheric uncertainties of the forecasting system (Yang et al., 2015a; Mu et al., 2018).

The following 6-hourly variables in each forecast were used to generate the fields to force the ice-ocean model: 2 m dew point temperature, 2 m temperature, 10 m surface winds, surface pressure, total cloud cover and total precipitation. There is no precipitation output at 0000 UTC, and an additional redistribution of the accumulated precipitation is needed to obtain the 6-hourly mean precipitation required by the model. Other necessary fields, which are not available in the TIGGE archive, are computed by formulas using existing data. The specific humidity is calculated from dew point temperature and surface pressure following Hess (1959). The downward shortwave radiation is calculated from dew point temperature, cloud and astronomical parameters according to Parkinson & Washington (1979). The downward longwave radiation is calculated based on 2 m temperature and cloud clover (Parkinson & Washington, 1979).

### 3.3 Satellite Data Assimilation

The Parallel Data Assimilation Framework (PDAF, Nerger & Hiller, 2013, `http://pdaf.awi.de`) is used for assimilating thickness and concentration data. For the sea ice thickness, the daily SMOS ice thickness data thinner than 1.0 m and the weekly mean

CryoSat-2 ice thickness data are assimilated simultaneously into the model as described in Mu et al. (2018).

The sea ice concentration data for data assimilation were processed at IFREMER and are provided by ICDC (`http://icdc.cen.uni-hamburg.de/`). The ARTIST Sea Ice (ASI) algorithm is applied to brightness temperatures measured with the 85 GHz SSM/I and/or SSM/IS channels (Kaleschke et al., 2001; Spreen et al., 2008). The 85 GHz channel is subject to the weather conditions. To reduce this influence, a 5-day median filter is applied to the data before publishing (Kern et al., 2010). The spatial resolution of the sea ice concentration data is 12.5 km $\times$ 12.5 km in a polar stereographic projection. Following Yang et al. (2016a, 2016b), a uniform constant value of 0.25 fractional sea ice area is assumed as observational uncertainties accounting for measurement and representation errors (Janjić et al., 2017) in the study.

A model ensemble (section 3.1) is driven by the atmospheric ensemble data sets derived from the UKMO ensemble forecasts to generate perturbed model states every day. The uncertainties in the model caused by parameters and imperfect physical processes are not considered explicitly (Shlyaeva et al., 2016). A variant of the ensemble Kalman filter, the local version of Error Subspace Transform Kalman Filter (LESTKF), is applied in the study. The LESTKF provides consistent projections between the ensemble space and the error subspace (Nerger et al., 2012), and outperforms the Local Singular Evolutive Interpolated Kalman filter (LSEIK) that was used in Mu et al. (2018). The sea ice concentration and the sea ice thickness form the state vector. In each analysis step, the LESTKF corrects the forecast state vector of each model in the ensemble taking into account the model uncertainties, which are calculated from the ensemble of model states, and the uncertainties of sea ice concentration and thickness. During this process, only satellite observations within a radius of 126 km around each model grid point are considered. This localization radius has been found optimal in Yang et al. (2014) and was also used in Mu et al. (2018). For the analysis step, the observations are weighted with distance from the grid point by a quasi-Gaussian weight function (Gaspari & Cohn, 1999). After the analysis step, the ensemble mean sea ice thickness can be thought of as combined dynamic model and satellite thickness (CMST) estimates. The reader is referred to Mu et al. (2018) for more details of the data assimilation procedure.

During the period without UKMO ensemble forcing data, the model is forced by the UKMO unperturbed forcing. Ensemble inflation, which is not necessary with the ensemble forcing, is achieved in the LESTKF with a forgetting factor of 0.97 (Yang et al., 2015a).

## 4 Results

We use the root-mean-square deviation (RMSD), the bias and the correlation coefficient as the evaluation metrics for comparing ice thickness data. The RMSD between two vectors $X$ and $Y$ is calculated as RMSD $= \sqrt{E[(X-Y)^2]}$, the bias ($B$) is calculated as B $= E[X-Y]$, and the correlation coefficient ($C$) of two vectors is calculated as C $= E[(X-EX)(Y-EY)]/(\sigma_x \sigma_y)$, where $E$ is the expectation operator, $\sigma_x$ and $\sigma_y$ are the standard deviations of the vectors $X$ and $Y$, respectively. The centered RMSD used for Taylor diagrams is CRMSD $=\sqrt{E[((X-EX)-(Y-EY))^2]}$. The standard deviations and the CRMSDs are then normalized by dividing with the standard deviations of the references, so that $(\mathrm{CRMSD}/\sigma_{\mathrm{ref}})^2 = (\sigma/\sigma_{\mathrm{ref}})^2 + 1 - 2\,\mathrm{C}\,\sigma/\sigma_{\mathrm{ref}}$ is always satisfied in the Taylor diagrams and all statistics for different references can be shown in the same plot. All statistics are calculated over the overlapped temporal and spatial coverage for different datasets.

Sea ice thickness estimates of each product in section 2 are restricted to the CryoSat-2 years 2010 to 2016 for all comparisons. For the comparisons with BGEP ice thickness, SMOS, CryoSat-2, CS2SMOS, PIOMAS, and CMST data are interpolated onto the locations of the three BGEP moorings. For the comparisons with IMB buoy thickness, the above datasets are interpolated onto the daily IMB buoy trajectories. IceBridge thickness and uncertainties are binned and averaged within each grid cell of our model before comparing.

### 4.1 Spatial Distribution of Ice Thickness

Arctic sea ice volume usually reaches its maximum in April in PIOMAS. Evaluating the spatial distributions of sea ice thickness during this maximum gives valuable insights into the resolved spatial variability of any sea ice product. The SMOS data, however, and consequently the CS2SMOS product do not cover the entire April, so that we use March sea ice thickness in each dataset for comparison instead.

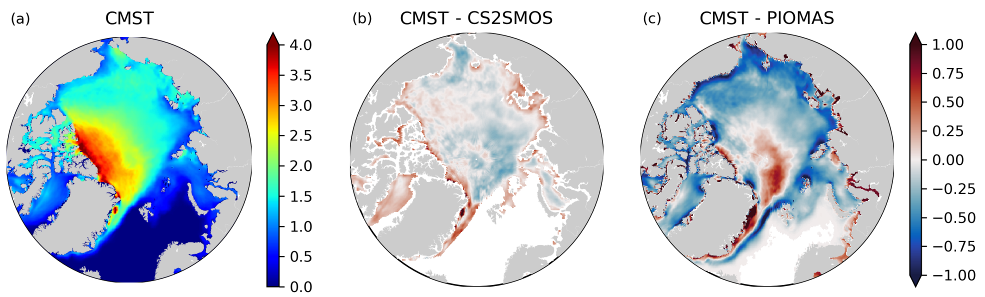


**Figure 1.** Comparison of sea ice thickness in March averaged from 2011 to 2016 between CMST, CS2SMOS, and PIOMAS. **(a)** CMST sea ice thickness (m) and **(b)** difference (m) between CMST and CS2SMOS, and **(c)** difference (m) between CMST and PIOMAS.

The March CMST averaged over the years 2011 to 2016 has a thickness below 1.5 m along the northern coast of the American Continent and over the Barents Sea, the Kara Sea, the Laptev Sea and the Baffin Bay (Figure 1a). The central Arctic is covered by thicker ice around 2.0 m with multi-year thick ice above 3.0 m north of the CAA. The RMSD of mean March sea ice thickness between CMST and CS2SMOS is 0.16 m (Figure 1b). CMST estimates thicker ice (deviations above 0.25 m) in the shallow Siberian Seas, north of the CAA and east of Greenland where the uncertainties of CS2SMOS are large (Ricker et al., 2017, their Figure 9). The detailed comparisons to in-situ observations of sea ice thickness north of the CAA and east of Greenland will be shown in section 4.2.3.

March CMST is generally thinner than PIOMAS thicknesses except along the east-coast of Greenland, north of Ellesmere Island, and parts of the transpolar drift close to Fram Strait (Figure 1c). Differences reach easily 0.5 m in the marginal ice area and in the shelf seas. The RMSD between CMST and PIOMAS is 0.41 m. Compared to ICESat ice thickness and in-situ ice thickness measurements, PIOMAS tends to overestimate the thin ice and underestimate the thick ice (Schweiger et al., 2011). Our results suggest that our data assimilated model corrects some of these biases present in PIOMAS.

The sea ice thickness frequency distributions of the CMST, CS2SMOS, and PIOMAS (Figure 2) support this impression. The thickness frequency distributions of CMST and CS2SMOS are very similar except for the thinnest category and the 1.0 - 1.5 m bin. Consequently the mean thickness of ice north of 65°N is almost exactly the same with 1.74 m (and equivalently volume of $13.7 \times 10^3\,\mathrm{km}^3$) for CMST and CS2SMOS. The similarity of these two estimates is not very surprising, because they both use the same SMOS and CryoSat-2 data. In PIOMAS, the mean thickness is 1.97 m and the ice volume is $15.48 \times 10^3\,\mathrm{km}^3$. The larger mean thickness is consistent with Figure 1c and also apparent in the ice thickness frequency distribution with more ice in thicker categories and less ice in thinner categories (Figure 2).

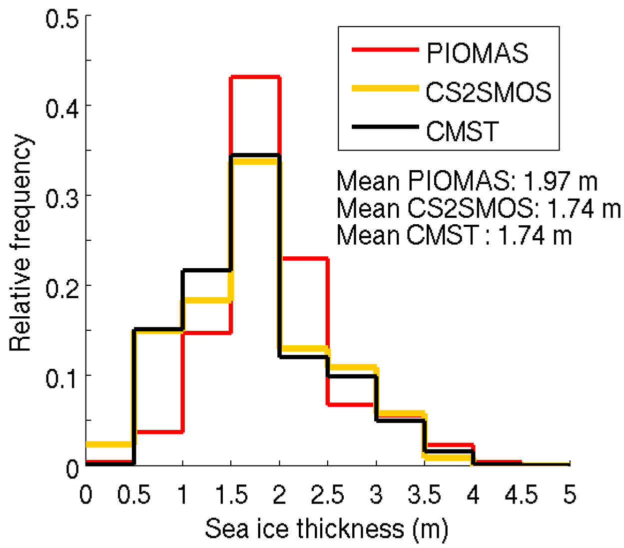


**Figure 2.** Histograms of sea ice thickness frequency distributions in March averaged from 2011 to 2016 for CMST (black), CS2SMOS (orange) and PIOMAS (red). The statistics are calculated over the overlapping area of the three datasets.

Climate models tend to underestimate extreme events (Flato et al., 2013), so that simulating the record minimum of Arctic sea ice extent in September 2012 represents a powerful benchmark test for any sea ice ocean model. The sea ice thickness fields in September 2012 (Figure 3) of CMST and PIOMAS have similar patterns, but for CMST the ice is generally thicker in the central Arctic and along the north coasts of Greenland and the CAA. Some of these systematic differences, for example in the central Arctic, can already be found in March (not shown, but Figure 1c shows the six-year average). The mean thickness, taking into account only ice thicker than 0.05 m, is 1.28 m for CMST and 0.77 m for PIOMAS. The gradients of sea ice thickness in the marginal ice area (Figure 3) are larger in CMST than in PIOMAS, that is, the thicker ice extends further into the

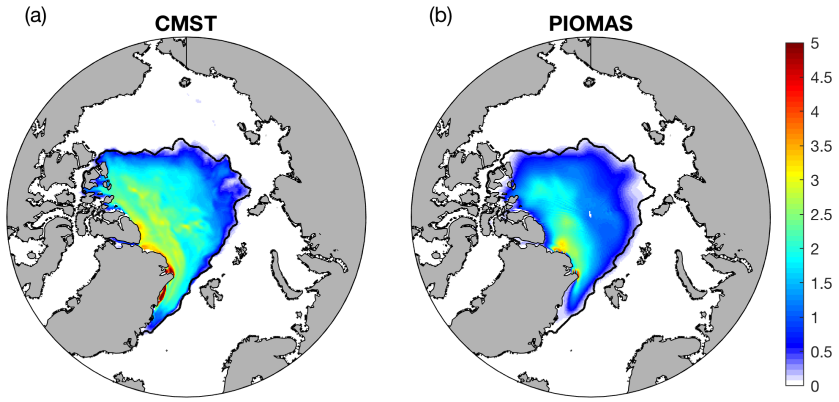


**Figure 3.** Sea ice thickness (m) in September 2012 for **(a)** CMST and **(b)** PIOMAS. Note that the black contoured line indicates sea ice concentration of 15% retrieved from AMSR-E using the Bootstrap algorithm by University of Bremen.

marginal ice zone. PIOMAS has a lower ice extent than the observations (Figure 3), although sea ice concentration data are also used to constrain the model. There are no independent thickness observations to decide which of these two thickness fields are more realistic, but the similar differences between ICESat and PIOMAS from October to November in the period 2003 to 2007 (Schweiger et al., 2011, their Figure 6) suggest that there is not enough ice in the PIOMAS solution. It is plausible that the thicker ice in March in CMST (Figure 1a), which is mainly due to the assimilation of CryoSat-2 data, preconditions the system to lead to thicker and hence more realistic ice in September.

## 4.2 Comparison with In-situ Observations

### *4.2.1 Comparison to BGEP ULS Data*

The annual cycle and the inter-annual variability of ice thickness are reproduced both in CMST and PIOMAS at all three mooring locations BGEP_A, BGEP_B and BGEP_D (Figure 4). As PIOMAS, the CMST estimate also reproduces the rapid decline of ice thickness during melt seasons, when no satellite thickness data are available. All data that went into CS2SMOS are also assimilated into CMST, so it is not surprising that CMST is closer to CS2SMOS than PIOMAS. When the satellite data do not agree with the in-situ ULS-data (e.g., in winter of 2012/2013 at BGEP_A, BGEP_B, and BGEP_D or in winter of 2013/2014 at BGEP_A), the CMST does neither and the PIOMAS thickness is closer to the in-situ data. At other times (e.g., most of the record in the freezing season) the satellite thickness corrects CMST and leads to a better fit to the in-situ data than those of PIOMAS thickness estimates. PIOMAS tends to have a positive bias relative to satellite thickness during ice growing periods. This is consistent with the finding that the initial growth rates in numerical models are generally too large compared to observations possibly because they are too sensitive to the demarcation thickness parameter $H_0$ (Johnson et al., 2012). The assimilation of ice thickness reduces the lower ice growth rate in CMST estimates. However, the satellite thickness assimilated in late April (e.g., in 2015 and 2016 at BGEP_B) also introduces biases, which leads the model to be not able to reach its annual thickness maximum.

CMST captures the high fluctuation of sea ice thickness at BGEP_A in 2014 (specifically the period marked in green in Figure 4) although with higher values compared to observations, while at BGEP_D, CMST reproduces too thick ice. This different behavior is because sea ice concentration and thickness are not correlated very well in nature over the melting hiatus periods. The assimilation will occasionally generate abnormal values of thickness in the marginal ice zones due to abrupt ice concentration increase triggered by wind convergence. In the absence of thickness data, ice thickness is still corrected by ice concentration data by means of the error-covariance between thickness and concentration. This covariance is approximated in LESTKF so that the CMST thickness during summer cannot be as reliable as in winter and biases can also develop. When thickness data become available again, these biases are quickly corrected. This is very obvious in the thickness time series in October, 2013 at BGEP_D. In 2014, ensemble forcing was not available from June to October. Interestingly, large summer biases develop that are probably caused by the suboptimal "ersatz" procedure of applying a forgetting factor (Yang et al., 2015a).

The fit of CMST, PIOMAS, and CS2SMOS to the BGEP ULS-data is summarized in Figure 5. At all three locations (BGEP_A, BGEP_B, BGEP_D), PIOMAS thickness correlates slightly better with the in-situ observations than CMST and CS2SMOS (Figures 5a and 5b). CMST correlates better with observations than CS2SMOS (Figure 5b). No product can reproduce the daily variability of the observed thickness shown in Figure 4, but the standard deviations of the PIOMAS estimates are closer to the observations (1.0 m) at all three locations.

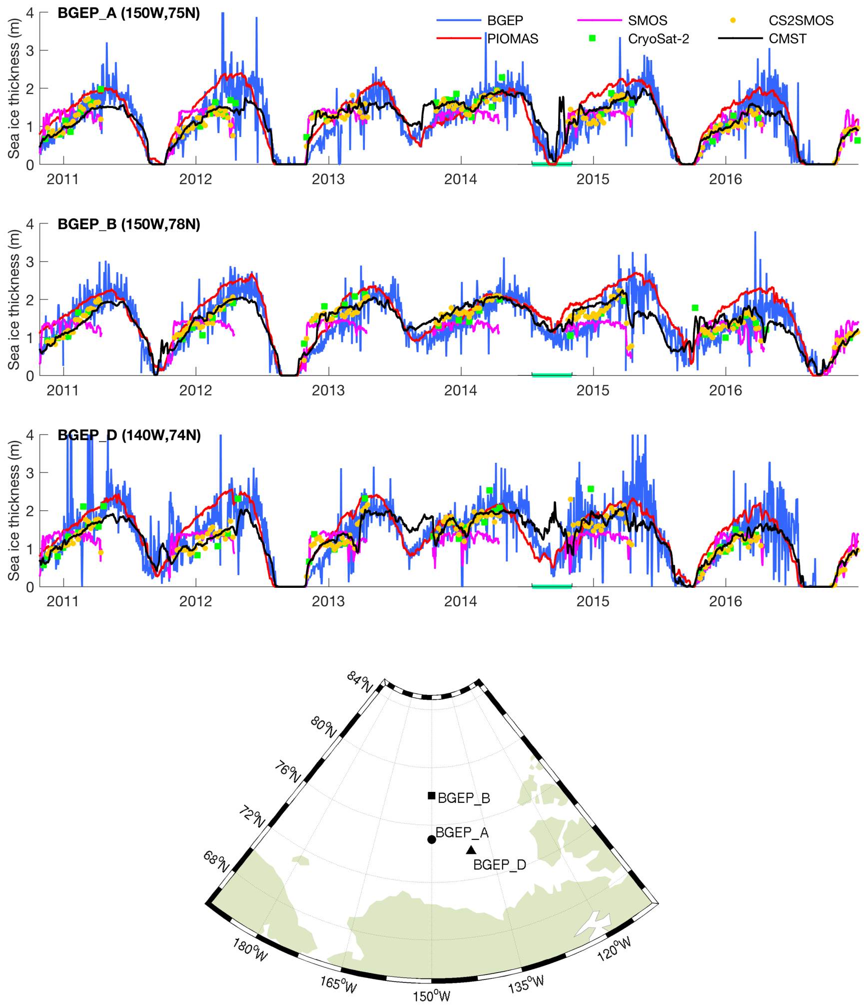


**Figure 4.** Time series of sea ice thickness (m) for BGEP ULS data (blue), SMOS (magenta), CS2SMOS (orange dot), PIOMAS (red), CryoSat-2 (green square), and CMST (black) at BGEP moorings BGEP_A, BGEP_B and BGEP_D. The short period without ensemble forcing for CMST is marked in green on the time axis. Locations of ULS moorings BGEP_A (75°N, 150°W), BGEP_B (78°N, 150°W) and BGEP_D (74°N, 140°W) are represented by dot (●), square (■) and triangle (▲), respectively.

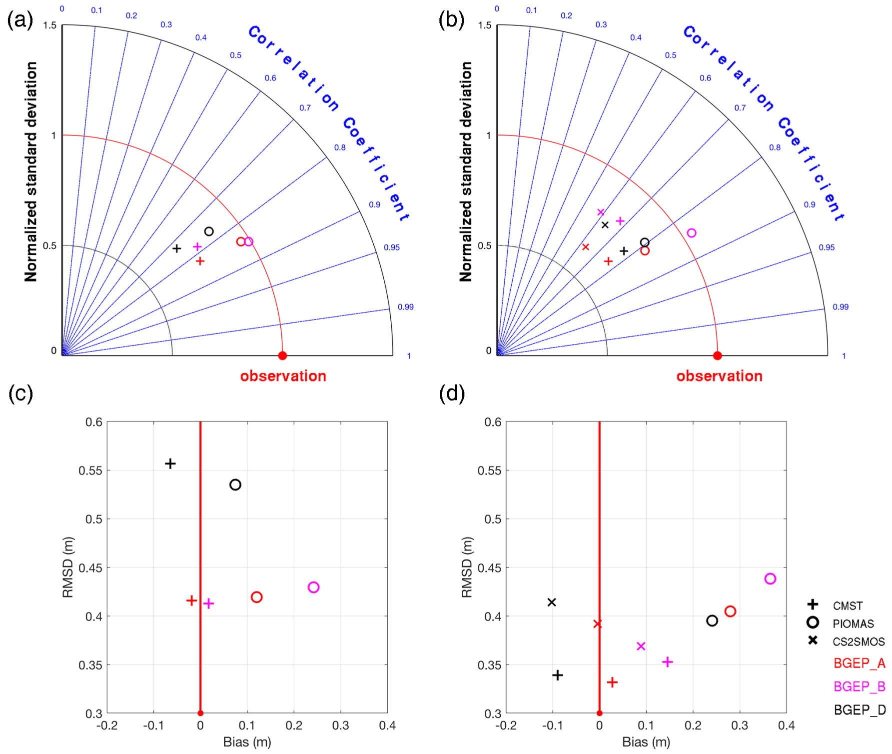


**Figure 5.** Normalized Taylor diagram (a, b) and RMSD versus bias (c, d) for CMST (+), PIOMAS (∘) and CS2SMOS (×) with respect to BGEP observations at BGEP_A (red), BGEP_B (magenta) and BGEP_D (black). **(a, c)** are computed over the period when BGEP ULS-data are avaiable and **(b, d)** are computed for the CS2SMOS period (i.e. without melting season). In Taylor diagrams the normalized standard deviation is on the radial axis and the correlation coefficient is on the angular axis. The observations are indicated by red dots.

The CMST biases relative to the ULS-data are smaller than for PIOMAS (Figures 5c and 5d). The positive biases of PIOMAS suggest that PIOMAS overestimates the thickness especially in the freezing season. The RMSD of PIOMAS thickness is a little smaller than for CMST at BGEP_D, when the summer season is included (Figure 5c), but much larger at BGEP_B (Figures 5c, 5d, and 4b). The biases of CMST and CS2SMOS are similar, but note that here CMST has a lower RMSD than CS2SMOS. Comparison between Figures 5c and 5d also suggests that larger deviations with respect to observations for CMST are mostly in the melting season, which can also be found directly in Figure 4.

#### *4.2.2 Comparison to IMB Buoy Data*

Lagrangian buoy data are very useful for studying local growth and melt processes together with 1-D column models of ice thermodynamics (e.g., Cheng et al., 2014). It is less straightforward to compare the grid averaged results of a Eulerian ice-ocean model to Lagrangian point observations. This is particularly true for sea ice thickness that is always subject to large scale dynamic deformation processes and/or local ridging. That the complex mixture of leads, first-year ice and multi-year ice often occur over distances of only tens of meters makes the situation even worse (Perovich & Richtermenge, 2006). Therefore we do not expect a very good agreement between gridded sea ice thickness variability and IMB buoys data along each trajectory.

Still, IMB buoy data provide information about temporal and spatial variability of sea ice thickness that can be used to evaluate model results given the appropriate metric. For our comparisons, we selected 32 IMB buoys with sufficiently long observation records during the period from October 2010 to December 2016. To improve the agreement between IMB buoy data and gridded products, the thickness biases can be adjusted in the buoy data to focus on the subsequent thickness evolutions (Lei et al., 2014). The underlying assumption is that the ice surface and oceanic heat flux are the same for the IMB buoy data and the gridded (model) data. This assumption works best when thermodynamic processes dominate and snow does not confound the heat balance. During initial inspection, we also found systematic differences between IMB buoy data, CMST and PIOMAS along the buoy trajectories. Figure 6 shows four selected cases that illustrate the systematic biases. These differences can be reduced by removing the mean thickness of each data set (not shown, but Figures 6a and d are obvious examples). Therefore, we compute the CRMSD, which removes the mean of time series, and the standard deviations of the time series, which measure the variability of sea ice thickness, as evaluation metrics. The metrics are summarized in Taylor diagrams (Figure 7).

In general, CMST standard deviations are closer to observations than PIOMAS standard deviations; the CRMSDs are also smaller for CMST, but PIOMAS correlates better with IMB buoy data (Figures 7a and 7c). The mean normalized standard deviation of CMST is 1.63, while that of PIOMAS is 2.00; the mean normalized CRMSD for CMST is 3.37 and that for PIOMAS is 3.63. The correlations for CMST and PIOMAS are 0.66 and 0.76, respectively. Some of these statistical differences between CMST and PIOMAS are expected, because the sea ice thickness assimilation adds information that should improve realism of the model on average, but at the same time can also introduce abrupt jumps when new data become available. Assimilating data that are not consistent with the model can hence lead to lower correlations. The better standard deviations of CMST suggest that CMST reproduces the thickness variability of IMB buoy data better than PIOMAS on longer time scales.

We now discuss four representative time series (Figure 6). Along the trajectories of buoys 2011J (Figure 6a, 8 months, August 2011 to May 2012) and 2013G (Figure 6d, 7 months, September 2013 to May 2014), CMST is mostly constrained by CryoSat-2 thickness data and hence close to CS2SMOS, but the IMB buoy data, as in many other cases not shown, implies much thicker ice. In these cases, we assume that the IMB buoy location on the floe does not necessarily represent a large spatial average and the mean cannot be compared to the gridded model data. Instead the buoy provides useful information on sea ice thickness evolution. The CRMSD of CMST with respect to 2011J is 0.13 m, while that of PIOMAS is 0.36 m. The PIOMAS thickness is larger than the estimates by CMST and satellite data and overestimates the trend in the buoy data. At buoy 2013G, CMST, PIOMAS and CS2SMOS are very similar. Still, the CRMSD of CMST with respect to 2013G is 0.11 m and that of PIOMAS is 0.25 m implying a slightly better thickness variability in CMST.

In some cases, the data assimilation rejects satellite thickness data that are inconsistent with the model dynamics. At buoy 2011K (Figure 6b, 7 months, August 2011 to April 2012), this happens between February 1st 2012 and April 1st 2012, when CrySat-2 thickness data tends to be too large. As a consequence, the CMST thickness, somewhat fortuitously, agrees better with the IMB buoy data than CS2SMOS and PIOMAS,

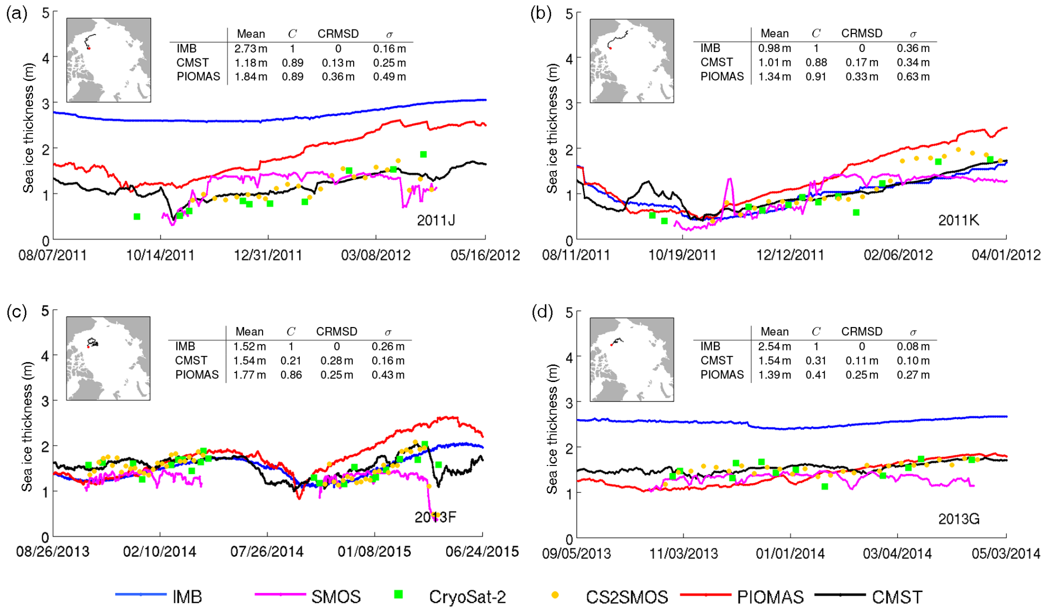


**Figure 6.** Sea ice thickness (m) time series: IMB buoy data (blue), SMOS (magenta), CryoSat-2 (green squares), CS2SMOS (orange dots), CMST (black), and PIOMAS (red) on each IMB buoys trajectory shown in the top left corner. The deployment location of the IMB is indicated by a red dot on the trajectory. The statistics for IMB buoy data, CMST, and PIOMAS are also shown in each plot. The date format is mm/dd/yyyy.

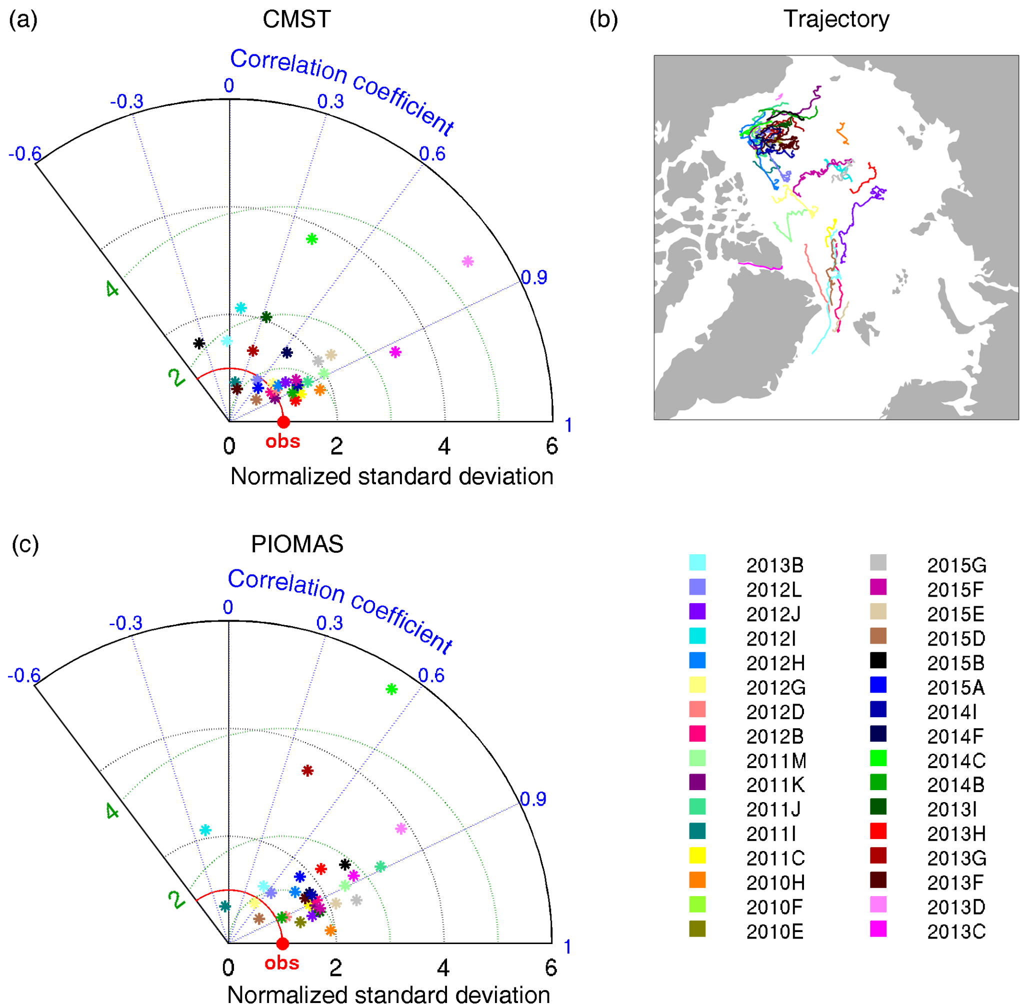


**Figure 7.** Taylor diagrams of **(a)** CMST and **(c)** PIOMAS with respect to all available IMB buoy data from October 2010 to December 2016. The green dotted lines indicate the normalized CRMSD. The trajectories of all the IMB buoys are shown in **(b)**. The reference observations are indicated by “obs” in red.

both of which also overestimate the thickness. In contrast, ice thickness in CMST is first too low and then becomes too large in September 2011, which we attribute to the assimilation of ice concentration with inaccurate covariances between thickness and concentration. Buoy 2013F (Figure 6c, 22 months, August 2013 to June 2015) recorded thickness for nearly two years. Both CMST and PIOMAS show plausible seasonal thickness variability, but PIOMAS tends to overestimate thickness after the summer of 2014 and the CMST thickness drops sharply in spring 2015 probably due to the impact of assimilating SMOS thickness data which also drops very quickly. The CRMSDs of CMST and PIOMAS are similar with values of 0.27 m and 0.24 m.

Another example of a strong jump in thickness in CMST can be found in 2011J in mid-October (Figure 6a). Here, the jump is associated with the availability of thickness data. During summer, the model without thickness assimilation (because there are no data available in summer) develops a bias and is inconsistent with the thickness data in October. Data assimilation quickly corrects this bias leading to the observed jump in the time series. This phenomenon can only be avoided by a data assimilation scheme that also takes into account future observations, for example a Kalman smoother (Evensen & Van Leeuwen, 2000), or full 4D-VAR state estimation as in ECCO (Forget et al., 2015).

#### *4.2.3 Comparison to Operation IceBridge Data*

The Operation IceBridge campaigns that are always conducted in March and April allow a meaningful comparison also to CS2SMOS. 31 airborne campaigns in 2011, 2012, and 2013 are selected for the comparison. Individual campaigns are short (order of hours), so that the variability along flight tracks represents spatial, but not temporal variability. In order to gain insight into spatial variations of different thickness products, the sections (e.g., Figure 8) are defined along the IceBridge trajectories without further taking into account the real flight routes in this study.

The general performance of the CMST, PIOMAS, CS2SMOS thickness datasets with respect to IceBridge thickness is summarized in Taylor plots (Figure 9). According to these metrics no dataset stands out clearly. CMST has the best average normalized standard deviation with 0.52 compared to PIOMAS (0.41) and CS2SMOS (0.48), but in all datasets the variability is smaller than in the observations. The mean normalized CRMSDs of 1.13 (CMST), 1.12 (PIOMAS), and 1.17 (CS2SMOA) are very simi-

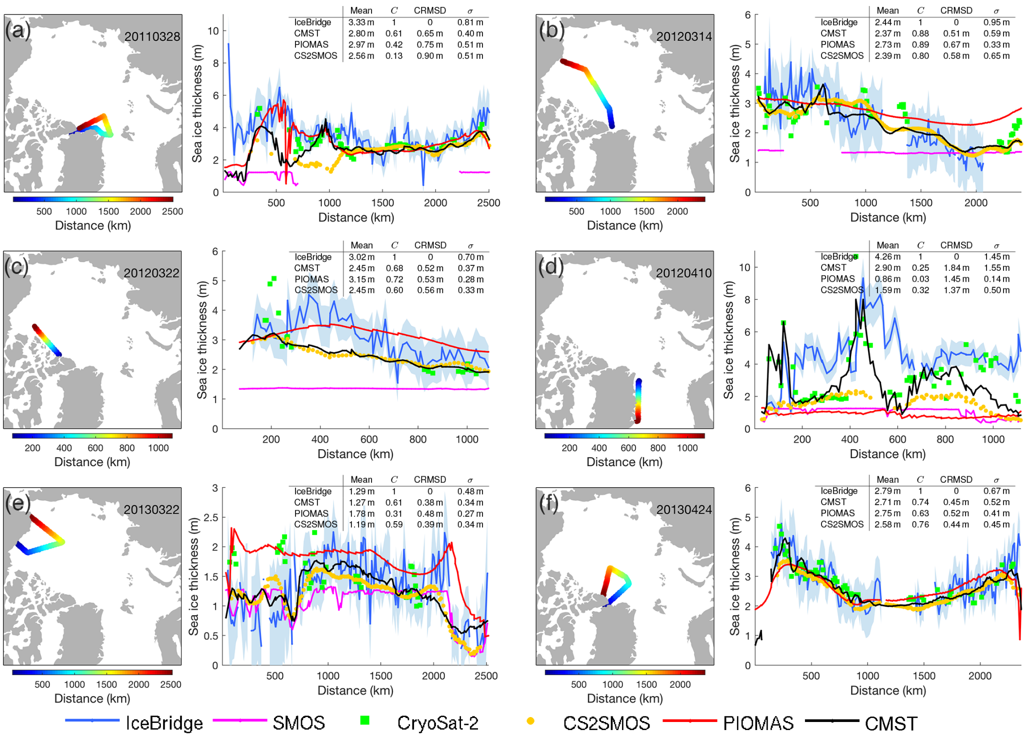


**Figure 8.** Sea ice thickness along Operation IceBridge trajectories. The trajectory of each campaign is shown on the map to the left of each plot, and colors indicate the distance from the starting point. The sea ice thickness of IceBridge (blue), SMOS (magenta), CryoSat-2 (green square), CS2SMOS (orange dot), PIOMAS (red) and CMST (black) in the right hand side plots are plotted against track distance. The shaded areas represent the uncertainties of IceBridge thickness as provided in the dataset. The statistics of IceBridge, PIOMAS, CMST and CS2SMOS sea ice thickness along the trajectories are also shown in each plot. Note that these statistics are computed over the overlapping periods of the four datasets.

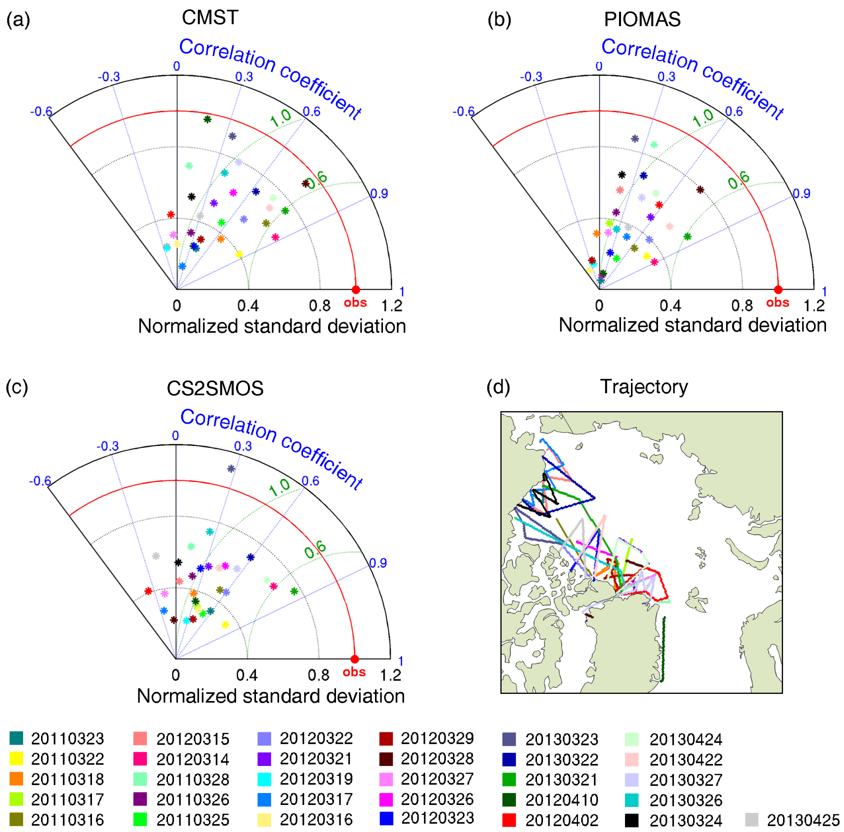


**Figure 9.** Taylor diagrams of **(a)** CMST, **(b)** PIOMAS and **(c)** CS2SMOS with respect to all IceBridge operations available in 2011, 2012 and 2013. The trajectories of all operations are shown in **(d)**. The green dotted lines indicate the normalized CRMSD. The reference observations are represented by "obs" in red. Note that the Taylor diagram of CS2SMOS is calculated over area where CS2SMOS thickness is available.

lar, with CMST and PIOMAS outperforming CS2SMOS slightly. In contrast to comparisons with BGEP ULS and IMB buoy data, where PIOMAS correlated best with observations, the CMST estimates have the best mean correlation of 0.40 with IceBridge measurements; the correlation coefficient is 0.35 for PIOMAS and 0.32 for CS2SMOS. In summary, the CMST agrees slightly better with the IceBridge thickness data than PIOMAS and CS2SMOS.

Of the 31 IceBridge campaigns in the study period, we discuss six representative examples (one in 2011, three in 2012, and two in 2013) in greater detail (Figure 8). Some of these selected sections (20110328, 20120314 and 20130424, Figures 8a, 8b and 8f) are repeat sections and others are focused on specific areas (20120322, 20120410 and 20130322, Figures 8c, 8d and 8e). Together, the selected sections illustrate all aspects of the performances of the different products.

Section 20130424 (Figure 8f) and the first 1000 km of 20120314 (Figure 8b) serve as examples of good agreement of CMST, PIOMAS, and CS2SMOS with IceBridge thickness estimates with maximum deviations of 0.25 m. Based on satellite data, CMST and CS2SMOS reproduce the transition from multi-year ice to first-year ice accurately along section 20120314 (Figure 8b). The same is true for the repeated section 20130321 one year later (not shown). In contrast, PIOMAS tends to overestimate the sea ice thickness in the thin ice area north of Alaska. In the following year, a similar PIOMAS bias is also found for section 20130322 in the Beaufort Sea (Figure 8e) (see also Schweiger et al., 2011; Johnson et al., 2012; Wang et al., 2016).

Some of the extreme thicknesses in the Nares Strait (Figure 8a), the Lincoln Sea (Figure 8f), and north of the CAA (Figure 8c) are not accurately represented in neither CMST, PIOMAS, or CS2SMOS. In these multi-year ice regions, the ice is heavily deformed and ridged, so that satellite observations are difficult: thin ice $< 1$ m, formed in leads opened by strong wind events, can be observed with SMOS and heavily ridged, thick multi-year ice with CryoSat-2 (Haas et al., 2006), so that conflicting thickness estimates in close proximity are possible. In combination, these data can lead to lower thicknesses as in CS2SMOS, or to some extent in CMST. In the Nares Strait (beginning of section 20110328 in Figure 8a), CMST clearly follows the SMOS thickness data, which is thinner by 3 m and more than the IceBridge estimate, because there is no CryoSat-2 data available to measure thick ice. Further, the resolution of the model (18 km) is not sufficient to resolve narrow straits accurately (we use 2 to 3 grid points across the Nares Strait), so that the model likely has a bias in this area anyway.

Guided by CryoSat-2 data, the thickness along the east coast of Greenland is best represented in CMST (Figure 8d). Both PIOMAS and CS2SMOS (probably due to the influence of SMOS data) strongly underestimate the thickness in this dynamical outflow region. The CMST is also too thin most of the time, but captures some of the variability and extreme thicknesses along the track. The PIOMAS thickness (like the SMOS thickness) is flat along this section and very thin.

## 5 Discussions

As shown above, our model ice thickness estimates are comparable to PIOMAS and fill the summer gaps of CS2SMOS. At the BGEP mooring, our CMST estimates agree better with CS2SMOS than the PIOMAS thickness, because the same thickness data was used in both estimates. Both ULS-data derived thickness and satellite derived thickness contain errors, but the satellite thickness assimilation further improves the model mean estimates at the cost of reduced variability and correlations. The better standard deviations and CRMSDs with respect to the IMB trajectories indicate that the CMST thickness agrees better with IMB data than the other datasets. All datasets can reproduce many aspects of the IceBridge thickness tracks, but none of the datasets represents ridged ice accurately. PIOMAS tends to overestimate the thickness in thin ice regions and appears to underestimate the spatial variability. In some places, where CS2SMOS does not compare well with IceBridge data because of conflicts between SMOS and CryoSat-2 data, the additional physics of the numerical model in CMST appears to reconcile these conflicts. The added value of thickness assimilation gives CMST an advantage over the model solution PIOMAS.

The model we used is forced by atmospheric ensemble forcing by which the uncertainties of air-sea or air-ice flux exchanges are explicitly estimated by the ocean ensemble. During the data assimilation, the ensemble spread will persist without the requirement of further applying the artificial inflation. Uncertainties of the CMST estimates can also be generated from the ensemble spread as a by-product.

The main limitation of the CMST estimates is that it relies heavily on the quality of satellite data products and the parameterizations of physical processes in the model.

The retrieval of CryoSat-2 thickness is based on the hydrostatic equilibrium assumption. Whether this is still appropriate in the ridged ice area along northern coast of CAA or in the fast ice area such as the Siberian Seas is still not clear. The validation of the snow thickness climatology used for CryoSat-2 thickness retrieval in recent years also needs further investigation. Satellite thickness data conflicts would lead to larger uncertainties in our final product. Examples of these conflicts can be found along the northern coast of Greenland where open water forms, east of Greenland where there are ice floes and in the Baffin Bay where snow climatology is not applicable for thickness retrieval.

In addition, the assimilation of sea ice concentration in the early freezing period in late summer will occasionally lead to unrealistically thick ice in marginal ice zones in the CMST estimates. This cannot be circumvented in the current implementation. A possible remedy may be applying a threshold to the thickness correction, but exploring the details of such an algorithm requires a dedicated investigation beyond the scope of our work.

In the Siberian Seas, the satellite thickness assimilation improves the ice thickness estimates of CMST over those of PIOMAS. Simulating the Siberian Seas with sea ice models without data assimilation requires the parameterization of land fast ice processes or modifications on ice ridging dynamics. In an evaluation of ice thickness by six models including the MITgcm in a very similar configuration, the models generally tend to overestimate the thickness in the regions of flat immobile landfast ice especially in the Siberian Seas (Johnson et al., 2012). These systematic errors are expected to persist because landfast ice is neither parameterized nor resolved in the model(s) (Lemieux et al., 2016). The CMST estimate appears to reject the satellite thickness in the Siberian Seas because of the large data uncertainties, but the model dynamics produce too thick sea ice. This bias may be alleviated by tuning or improving the ice strength and ridging parameterization. In our setup, ridging is parameterized by restricting sea ice fractional area to values $\leq 1$ (Schulkes, 1995). Model parameters such as albedo, compressive strength, demarcation thickness $H_0$ for lead closing, etc. will also play a big part in simulating thickness variations and spatial distributions, particularly when satellite thickness is unavailable in melt seasons. These parameters are currently not well constraint. Therefore, uncertainties of the CMST estimates also result from potentially incomplete parameterizations of physical processes in the model. The effects of parameter choices are ignored in this study.

The comparison of model and data products also provides some insight into the uncertainties in different ice thickness measurements. The deviations between the satellite thickness and ULS in late April (Figure 4) imply that more cross validations are necessary to improve thickness retrievals. Comparing IMBs (or Lagragian data in general) to large-scale models is delicate and requires a careful evaluation of the data on Eulerian grids. Still, a distributed network of IMBs may provide an opportunity to assess the performances of different data products. The near-future Multidisciplinary drifting Observatory for the Study of Arctic Climate (MOSAiC; `http://www.mosaicobservatory.org/`) is expected to conduct such observations. Uncertainties of IceBridge thickness stem from uncertainties in snow detection and spatially and temporally varying ice and snow densities (Kurtz et al., 2013). The IceBridge footprint is only 40 m. In this way thickness data statistics are biased in the along track direction and cannot take into account the cross track variability. In contrast, the smallest model element is a grid cell with cell width ˜18 km.

## 6 Conclusions

Daily entire Arctic sea ice thickness estimates are obtained from combining remotely sensed sea thickness and concentration data with a sea ice-ocean model. These thickness estimates are available at all times for the entire CryoSat2-period 2010–2016 closing the satellite thickness observation gap in summer with the help of model dynamics and concentration data assimilation. The additional thickness data in combination with a sophisticated data assimilation scheme helps to reduce biases that are still present in current sea ice thickness products. The generated CMST estimates that take advantage of satellite thickness observations and physics of the sea ice-ocean model can be viewed as an optimal compromise between CS2SMOS and PIOMAS insofar as it combines the strengths of both products (thickness observations and model dynamics).

Our main findings are that the CMST is relatively close to the CS2SMOS data, which is not surprising as both use the same thickness data. The thickness data help to reduce some biases present in other models, but in general the comparison with in-situ thickness data turns out to be similar to that of PIOMAS thickness to in-situ data. Because we use a model, the thickness estimates can be extended into the summer season, where adequate initial conditions together with appropriate surface forcing help to simulate realistic summer sea ice thicknesses.

The new Arctic sea ice thickness estimate CMST provides an opportunity to study the ice volume changes in recent years. The difference maps between CMST and PIOMAS suggest areas where more in-situ sea ice thickness measurements would help reconcile the models with data. Moreover, we expect that this dataset will serve as a good reference for parameterizations for sea ice models.

**Acknowledgments**

We thank Ruibo Lei from the Polar Research Institute of China for the discussions about the data processing of the IMB buoys, Jinlun Zhang from the University of Washington for providing the PIOMAS sea ice thickness data and Xi Liang from National Marine Environmental Forecasting Center for the suggestions on sea ice assimilation. We thank the University of Hamburg for providing SMOS sea ice thickness data and the ASI-SSMI sea ice concentration data, National Snow and Ice Data Center (NSIDC) for providing the IceBridge thickness data, the Woods Hole Oceanographic Institution for the sea ice draft data, the Cold Regions Research and Engineering Laboratory for IMB data, and the European Centre for Medium-Range Weather Forecasts for the UKMO ensemble forecasting data. This study is supported by the National Natural Science Foundation of China (41706224, 41776192), the BMBF (Federal Ministry of Education and Research, Germany)-SOA (State Oceanic Administration, China) Joint Project (01DO14002) and the Federal Ministry of Education and Research of Germany in the framework of SSIP (grant01LN1701A). Contribution by SNL is partly made in the framework of the state assignment of FASO Russia (theme No. 0149-2018-0014) and the BMBF ERA-Net project EXOSYSTEM (grant 01DJ16016). The CMST data in this paper are archived in PANGAEA and available at https://doi.pangaea.de/10.1594/PANGAEA.891475.

## References

Bowler, N. E., Arribas, A., Mylne, K. R., Robertson, K. B., & Beare, S. E. (2008). The MOGREPS short-range ensemble prediction system. *Quart. J. Roy. Meteor. Soc.*, *134*(632), 703–722. doi: 10.1002/qj.234

Brodzik, M. J., Billingsley, B., Haran, T., Raup, B., & Savoie, M. H. (2012). EASE-Grid 2.0: Incremental but significant improvements for earth-gridded data sets. *ISPRS Int. J. Geo-Information*, *1*(3), 32–45. doi: 10.3390/ijgi1010032

Cheng, B., Vihma, T., Rontu, L., Kontu, A., Duguay, H. K. P. C., & Pulliainen, J.

(2014). Evolution of snow and ice temperature, thickness and energy balance in Lake Orajärvi, northern Finland. *Tellus A*, *66*(1).

Day, J. J., Hawkins, E., & Tietsche, S. (2014). Will Arctic sea ice thickness initialization improve seasonal forecast skill? *Geophys. Res. Lett.*, *41*, 7566–7575. doi: 10.1002/2014GL061694

Evensen, G., & Van Leeuwen, P. J. (2000). An ensemble kalman smoother for nonlinear dynamics. *Monthly Weather Review*, *128*(6), 1852–1867.

Flato, G., Marotzke, J., Abiodun, B., Braconnot, P., Chou, S., Collins, W., … others (2013). *Climate change 2013: The physical science basis. contribution of working group i to the fifth assessment report of the intergovernmental panel on climate change, chap. evaluation of climate models, 126 pp.* Cambridge University Press, Cambridge, United Kingdom and New York, NY, USA.

Forget, G., Campin, J., Heimbach, P., Hill, C., Ponte, R., & Wunsch, C. (2015). Ecco version 4: An integrated framework for non-linear inverse modeling and global ocean state estimation. *Geoscientific Model Development*, *8*(10), 3071–3104. doi: 10.5194/gmd-8-3071-2015

Francis, J. A., Chan, W., Leathers, D. J., Miller, J. R., & Veron, D. E. (2009). Winter Northern Hemisphere weather patterns remember summer Arctic sea-ice extent. *Geophys. Res. Lett.*, *36*(7). doi: 10.1029/2009GL037274

Gaspari, G., & Cohn, S. E. (1999). Construction of correlation functions in two and three dimensions. *Quart. J. Roy. Meteor. Soc.*, *125*, 723–757.

Haas, C., Hendricks, S., & Doble, M. (2006). Comparison of the sea-ice thickness distribution in the lincoln sea and adjacent arctic ocean in 2004 and 2005. *Annals of glaciology*, *44*, 247–252.

Haine, T. W., Curry, B., Gerdes, R., Hansen, E., Karcher, M., Lee, C., … others (2015). Arctic freshwater export: Status, mechanisms, and prospects. *Global and Planetary Change*, *125*, 13–35.

Hess, S. L. (1959). *Introduction to theoretical meteorology.* New York, NY: Holt, Rinehart, and Winston.

Hibler III, W. (1979). A dynamic thermodynamic sea ice model. *Journal of Physical Oceanography*, *9*(4), 815–846.

Janjić, T., Bormann, N., Bocquet, M., Carton, J., Cohn, S., Dance, S., … others (2017). On the representation error in data assimilation. *Quarterly Journal of the*

*Royal Meteorological Society*.

Johnson, M., Proshutinsky, A., Aksenov, Y., Lindsay, A. T. N. R., Haas, C., Zhang, J., … de Cuevas, B. (2012). Evaluation of Arctic sea ice thickness simulated by Arctic Ocean Model Intercomparison Project models. *J. Geophys. Res.*, *117*(C00D13). doi: 10.1029/2011JC007257

Kaleschke, L., Lüpkes, C., Vihma, T., Haarpaintner, J., Bochert, A., Hartmann, J., & Heygster, G. (2001). SSM/I sea ice remote sensing for mesoscale ocean-atmosphere interaction analysis. *Can. J. Remote Sens.*, *27*(5), 526–537. doi: 10.1080/07038992.2001.10854892

Kern, S., Kaleschke, L., & Spreen, G. (2010). Climatology of the nordic (Irminger, Greenland, Barents, Kara and White/Pechora) Seas ice cover based on 85 GHz satellite microwave radiometry: 1992-2008. *Tellus A*, *62*(4), 411–434. doi: 10.1111/j.1600-0870.2010.00457.x

Kumar, A., Perlwitz, J., Eischeid, J., Quan, X., Xu, T., Zhang, T., … Wang, W. (2010). Contribution of sea ice loss to Arctic amplification. *Geophys. Res. Lett.*, *37*(21). doi: 10.1029/2010GL04502

Kurtz, N., Farrell, S., Studinger, M., Galin, N., Harbeck, J., Lindsay, R., … Sonntag, J. (2013). Sea ice thickness, freeboard, and snow depth products from operation icebridge airborne data. *The Cryosphere*, *7*(4), 1035–1056. doi: 10.5194/tc-7-1035-2013

Kurtz, N., Studinger, M., Harbeck, J., Onana, V., & Yi, D. (2015). Icebridge l4 sea ice freeboard, snow depth, and thickness, version 1. *NASA National Snow and Ice Data Center Distributed Active Archive Center, Boulder, Colorado, USA*.

Kwok, R., Cunningham, G. F., Wensnahan, M., Rigor, I., Zwally, H. J., & Yi, D. (2009). Thinning and volume loss of the Arctic Ocean sea ice cover: 2003-2008. *J. Geophys. Res.*, *114*(7). doi: 10.1029/2009JC005312

Laxon, S. W., Giles, K. A., Ridout, A. L., Wingham, D. J., Willatt, R., Cullen, R., … Davidson, M. (2013). Cryosat-2 estimates of Arctic sea ice thickness and volume. *J. Geophys. Res.*, *40*(4), 732–737. doi: 10.1002/grl.50193

Lei, R., Li, N., Heil, P., Cheng, B., Zhang, Z., & Sun, B. (2014). Multiyear sea ice thermal regimes and oceanic heat flux derived from an ice mass balance buoy in the Arctic Ocean. *J. Geophys. Res.*, *119*(1), 537–547. doi: 10.1002/2012JC008731

Lemieux, J.-F., Dupont, F., Blain, P., Roy, F., Smith, G. C., & Flato, G. M. (2016). Improving the simulation of landfast ice by combining tensile strength and a parameterization for grounded ridges. *Journal of Geophysical Research: Oceans*, *121*(10), 7354–7368.

Lisæter, K. A., Evensen, G., & Laxon, S. W. (2007). Assimilating synthetic cryosat sea ice thickness in a coupled ice-ocean model. *J. Geophys. Res.*, *112*(7), 1–14. doi: 10.1029/2006JC003786

Liu, J., Curry, J. A., Wang, H., Song, M., & Horton, R. M. (2012). Impact of declining arctic sea ice on winter snowfall. *Proc. Nat. Acad. Sci. USA*, *109*(11), 4074–4079. doi: 10.1073/pnas.1114910109

Losch, M., Menemenlis, D., Campin, J.-M., Heimbach, P., & Hill, C. (2010). On the formulation of sea-ice models. Part 1: Effects of different solver implementations and parameterizations. , *33*(1–2), 129–144. doi: 10.1016/j.ocemod.2009.12.008

Marshall, J., Adcroft, A., Hill, C., Perelman, L., & Heisey, C. (1997). A finite-volume, incompressible Navier Stokes model for studies of the ocean on parallel computers. *J. Geophys. Res.*, *102*(C3), 5753–5766. doi: 10.1029/96JC02775

Melling, H., Johnston, P., & Riedel, D. (1995). Measurements of the underside topography of sea ice by moored subsea sonar. *J. Atmos. Oceanic Technol.*, *12*(3), 589–602.

Menemenlis, D., Campin, J.-M., Heimbach, P., Hill, C., Lee, T., Nguyen, A., ... Zhang, H. (2008). Ecco2: High resolution global ocean and sea ice data synthesis. *Mercator Ocean Quarterly Newsletter*, *31*, 13–21.

Mu, L., Yang, Q., Losch, M., Losa, S. N., Nerger, L., Ricker, R., & Liang, X. (2018). Improving sea ice thickness estimates by assimilating CryoSat-2 and SMOS sea ice thickness data simultaneously. *Quart. J. Roy. Meteor. Soc.*. doi: 10.1002/qj.3225

Mu, L., Zhao, J., & W., Z. (2017). Regime shift of the dominant factor for halocline depth in the Canada Basin during 19902008. *Acta Oceanol. Sin.*, *36*(1), 35–43. doi: 10.1007/s13131-016-0883-0

Nerger, L., & Hiller, W. (2013). Software for ensemble-based data assimilation systems – implementation strategies and scalability. *Comput. Geosci.*, *55*, 110–118. doi: 10.1016/j.cageo.2012.03.026

Nerger, L., Janji, T., Schrter, J., & Hiller, W. (2012). A unification of ensemble square root kalman filters. *Monthly Weather Review*, *140*(7), 2335-2345.

Nguyen, A. T., Menemenlis, D., & Kwok, R. (2011). Arctic ice-ocean simulation with optimized model parameters: Approach and assessment. *J. Geophys. Res.*, *116*(C4). doi: 10.1029/2010JC006573

Overland, J. E., & Wang, M. (2010). Large-scale atmospheric circulation changes are associated with the recent loss of Arctic sea ice. *Tellus A*, *62*(1), 1–9. doi: 10.1111/j.1600-0870.2009.00421.x

Parkinson, C. L., & Washington, W. M. (1979). A large-scale numerical model of sea ice. *Journal of Geophysical Research: Oceans*, *84*(C1), 311–337.

Perovich, D., Richter-Menge, J., Elder, B., Arbetter, T., Claffey, K., & Polashenski, C. (2009). Observing and understanding climate change: Monitoring the mass balance, motion, and thickness of arctic sea ice. *URL http://imb. crrel. usace. army. mil, URL http://imb. crrel. usace. army. mil*.

Perovich, D., & Richtermenge, J. A. (2006). From points to poles: extrapolating point measurements of sea-ice mass balance. *Annals of Glaciology*, *44*(1), 188-192.

Richter-Menge, J. A., Perovich, D. K., Elder, B. C., Claffey, K., Rigor, I., & Ortmeyer, M. (2006). Ice mass-balance buoys: A tool for measuring and attributing changes in the thickness of the arctic sea ice cover. *Ann. Glaciol.*, *44*, 205–210.

Ricker, R., Hendricks, S., Helm, V., Skourup, H., & Davidson, M. (2014). Sensitivity of CryoSat-2 Arctic sea ice freeboard and thickness on radar-waveform interpretation. *The Cryosphere*, *8*(4), 1607–1622. doi: 10.5194/tc-8-1607-2014

Ricker, R., Hendricks, S., Kaleschke, L., Tian-Kunze, X., King, J., & Haas, C. (2017). A weekly Arctic sea-ice thickness data record from merged CryoSat-2 and SMOS satellite data. *The Cryosphere*, *11*, 1607–1623. doi: 10.5194/tc-11-1607-2017

Schulkes, R. (1995). A note on the evolution equations for the area fraction and the thickness of a floating ice cover. *Journal of Geophysical Research: Oceans*, *100*(C3), 5021–5024.

Schweiger, A., Lindsay, R., Zhang, J., Steele, M., Stern, H., & Kwok, R. (2011). Uncertainty in modeled Arctic sea ice volume. *J. Geophys. Res.*, *116*(9). doi: 10.1029/2011JC007084

Semtner Jr, A. J. (1976). A model for the thermodynamic growth of sea ice in numerical investigations of climate. *Journal of Physical Oceanography*, *6*(3), 379–

389.

Serreze, M. C., Holland, M., & Stroeve, J. C. (2007). Perspectives on the Arctics shrinking sea-ice cover. *Science*, *315*, 1533–1536. doi: 10.1126/science.1139426

Shlyaeva, A., Buehner, M., Caya, A., Lemieux, J.-F., Smith, G. C., Roy, F., … Carrieres, T. (2016). Towards ensemble data assimilation for the Environment Canada Regional Ice Prediction System. *Quart. J. Roy. Meteor. Soc.*, *142*, 1090–1099. doi: 10.1002/qj.2712

Shutts, G. (2005). A kinetic energy backscatter algorithm for use in ensemble prediction systems. *Quart. J. Roy. Meteor. Soc.*, *131*, 3079–3102. doi: 10.1256/qj.04.106

Smith, W. H. F., & Sandwell, D. T. (1997). Global seafloor topography from satellite altimetry and ship depth soundings. *Science*, *277*, 1957–1962. doi: 10.1126/science.277.5334.1956

Spreen, G., Kaleschke, L., & Heygster, G. (2008). Sea ice remote sensing using AMSR-E 89-GHz channels. *J. Geophys. Res.*, *113*(2). doi: 10.1029/2005JC003384

Tian-Kunze, X., Kaleschke, L., Maaß, N., Mäkynen, M., Serra, N., Drusch, M., & Krumpen, T. (2014). SMOS-derived thin sea ice thickness: Algorithm baseline, product specifications and initial verification. *The Cryosphere*, *8*(3), 997–1018. doi: 10.5194/tc-8-997-2014

Ungermann, M., Tremblay, L. B., Martin, T., & Losch, M. (2017). Impact of the ice strength formulation on the performance of a sea ice thickness distribution model in the arctic. *Journal of Geophysical Research: Oceans*, *122*(3), 2090–2107.

Wang, X., Key, J., Kwok, R., & Zhang, J. (2016). Comparison of Arctic sea ice thickness from satellites, aircraft, and PIOMAS data. *Remote Sens.*, *8*(9). doi: 10.3390/rs8090713

Wingham, D. J., Francis, C. R., Baker, S., Bouzinac, C., Brockley, D., Cullen, R., … Wallis, D. W. (2006). Cryosat: A mission to determine the fluctuations in Earths land and marine ice fields. *Adv. Sp. Res.*, *37*(4), 841–871. doi: 10.1016/j.asr.2005.07.027

Xie, J., Counillon, F., Bertino, L., Tian-Kunze, X., & Kaleschke, L. (2016). Benefits of assimilating thin sea ice thickness from SMOS into the TOPAZ system. *The Cryosphere*, *10*, 2745–2761. doi: 10.5194/tc-10-2745-2016

Yang, Q., Losa, S. N., Losch, M., Jung, T., & Nerger, L. (2015a). The role of atmospheric uncertainty in arctic summer sea ice data assimilation and prediction. *Quarterly Journal of the Royal Meteorological Society*, *141*(691), 2314–2323.

Yang, Q., Losa, S. N., Losch, M., Liu, J., Zhang, Z., Nerger, L., & Yang, H. (2015b). Assimilating summer sea-ice concentration into a coupled ice–ocean model using a lseik filter. *Annals of Glaciology*, *56*(69), 38–44.

Yang, Q., Losa, S. N., Losch, M., Tian-Kunze, X., Nerger, L., Liu, J., … Zhang, Z. (2014). Assimilating SMOS sea ice thickness into a coupled ice-ocean model using a local SEIK filter. *J. Geophys. Res.*, *119*(10), 6680–6692. doi: 10.1002/2014JC009963

Yang, Q., Losch, M., Losa, S. N., Jung, T., Nerger, L., & Lavergne, T. (2016a). Brief communication: The challenge and benefit of using sea ice concentration satellite data products with uncertainty estimates in summer sea ice data assimilation. *The Cryosphere*, *10*(2), 761–774. doi: 10.5194/tc-10-761-2016

Yang, Q., Losch, M., Loza, S., Jung, T., & Nerger, L. (2016b). Taking into account atmospheric uncertainty improves sequential assimilation of SMOS sea ice thickness data in an ice-ocean model. *J. Atmos. Oceanic Technol.*, *33*, 397–407. doi: 10.1175/JTECH-D-15-0176.1

Zhang, J., & Hibler, W. D., III. (1997). On an efficient numerical method for modeling sea ice dynamics. *J. Geophys. Res.*, *102*(C4), 8691–8702. doi: 10.1029/96JC03744

Zhang, J., Hibler, W. D., III, Steele, M., & Rothrock, D. A. (1998). Arctic ice-ocean modeling with and without climate restoring. , *28*(2), 191–217.

Zhang, J., & Rothrock, D. A. (2003). Modeling global sea ice with a thickness and enthalpy distribution model in generalized curvilinear coordinates. , *131*(5), 845–861. doi: 10.1175/1520-0493(2003)131⟨0845:MGSIWA⟩2.0.CO;2